

Analysis of Fracture Behavior of Ceramics by Generalized Multimodal Weibull Function

Yohtarō MATSUO, Kouichi YASUDA and Shiushichi KIMURA
Department of Inorganic Materials, Tokyo Institute of
Technology, Ookayama2-12-1, Meguro-ku, Tokyo, Japan

ABSTRACT

A new concept-generalized multimodal Weibull function-is presented based on the competing risk theory and fracture mechanics. As the case which has only one random variable, the distribution functions of fast-fracture strength, dynamic fatigue strength and cyclic fatigue life are reviewed. As a two-variable case, the distribution functions of fracture location and crack size at fracture origin are showed using the joint probability density function with respect to fracture stress and fracture location for n fracture causes with experimental verification on HP-Si₃N₄. The newly developed theory, which involves 3 random variables-fracture stress, fracture location and flaw orientation-is outlined. The method for estimating Weibull parameters, which is called as the multistep maximum likelihood method, is reviewed.

1. Introduction

Since almost all ceramics are polycrystalline made by sintering process, they involve many kinds of flaws in their surfaces and inside the bodies.

Flaws which may cause fracture can be divided into three categories as follows:

- (A) intrinsic flaws
- (B) coalescing microcracks
- (C) voids, flaws developed from voids.

In low and medium temperature ranges ($T < 0.5T_m$, T_m :melting

temperature), flaws (A) and (B) are predominant; the stress-strain relation is elastic up to fracture and strength being constant against temperature change. In high temperature ranges ($T > 0.5T_m$), flaws (C) are predominant, the stress-strain relation is nonlinear, and strength decreases as temperature increases.

Of the three categories of major flaws that influence the strength of structural ceramics, intrinsic flaws are the most important. They can further be divided as follows:

- internal flaws: pores, pore clusters, coarse grains, inclusions, internal cracks, weak grain boundaries
- surface flaws: cracks caused by machining or impact damage, exposed internal flaws

When ceramic materials are subjected to some kinds of loads under a definite environment, these intrinsic flaws 'compete' each other and the most hazardous flaw of them acts as a fracture origin which leads to final fracture.

In this review, we suggest that the fracture behaviors of ceramics under some conditions can be described by generalized multimodal Weibull function. Also we suggest how important the data of fracture causes are for estimating the Weibull parameters.

2. Generalized multimodal Weibull Function

According to the competing risk theory with independent risks[1], the probability density function of random variable X involving k fracture causes can be formulated by the following equation;

$$f(X) = \prod_{i=1}^k R_i \cdot \sum_{j=1}^k \lambda_j \quad (1)$$

where R_i and λ_j are the reliability function (or survival probability function) and the failure rate of i -th (or j -th) cause of fracture, respectively. We must note that the random variable X in Eq.(1) may be a vector; namely, Eq.(1) may be a multi-variable joint probability density function. We call Eq.(1) as the generalised multimodal Weibull function as long as the strength (or life-time) distribution derived from Eq.(1), as a marginal, is a multimodal (or uni-modal) Weibull distribution function.

In the following we discuss about some probability density functions or probability distribution functions in those cases which involve up to 3 random variables.

2.1 One-variable case

Fast fracture strength

According to the weakest link theory, the distribution function of the fast-fracture strength (σ_m) must obey so-called multimodal Weibull distribution function, which was derived from a competing risk model expressed by Eq.(1), written as

$$f(\sigma_m) = \sum_{i=1}^k B_i \cdot \exp\left[-\sum_{i=1}^k B_i\right] \quad (2)$$

where B_i : risk of rupture due to the i -th fracture cause and k : number of different fracture causes.

Now let us suppose that a test piece has a stress gradient and internal ($i=1$), surface ($i=2$) and edge ($i=3$) cracks for fracture causes. Then, for uniaxial Weibull distribution functions (functions applicable to uniaxial stress), we have B_i as follows:

$$B_1 = \int_V \left(\frac{\sigma - \sigma_{u1}}{\sigma_{o1}}\right)^{m_1} dV, \quad B_2 = \int_A \left(\frac{\sigma - \sigma_{u2}}{\sigma_{o2}}\right)^{m_2} dA, \quad B_3 = \int_L \left(\frac{\sigma - \sigma_{u3}}{\sigma_{o3}}\right)^{m_3} dL \quad (3)$$

where dV, dA and dL are nondimensional volume, surface, and line elements, respectively, and $m_i, \sigma_{oi}, \sigma_{ui}$ are Weibull parameters.

Also, for distribution functions applicable to the multiaxial stress state (multiaxial distribution function), B_i is given by [2]

$$B_1 = \frac{2}{\pi} \int_V \int_0^{\frac{\pi}{2}} \int_0^{\frac{\pi}{2}} \left(\frac{Z_1 - \sigma_{n1}}{\sigma_{01}} \right)^{m_1} \cdot Y(Z_1, \sigma_{n1}) \sin \varphi \, d\varphi \, d\theta \, dV$$

$$B_2 = \frac{2}{\pi} \int_A \int_0^{\frac{\pi}{2}} \left(\frac{Z_2 - \sigma_{n2}}{\sigma_{02}} \right)^{m_2} \cdot Y(Z_2, \sigma_{n2}) \, d\theta \, dA$$

$$B_3 = \int_L \left(\frac{Z_3 - \sigma_{n3}}{\sigma_{03}} \right)^{m_3} \cdot Y(Z_3, \sigma_{n3}) \, dL \quad (4)$$

where Z_i is a quantity derived from unstable crack extension conditions in a mixed mode and called an equivalent normal stress, and defined by

$$Z_i = \frac{K_{Ic}}{Y_i \sqrt{\pi c}} \quad (5)$$

where c : representative crack length, K_{Ic} : fracture toughness and Y_i : geometric constant. Equation (4) is very useful for designing brittle-structural components based on statistical analysis. We can also estimate the brittle fracture loci under biaxial or triaxial stress states (see Fig.1)[3,4] and the fracture behavior of ceramics with ground surfaces (see Fig.2)[5,6].

Dynamic fatigue strength and cyclic fatigue life

Assuming that the following slow crack growth law is dominant in almost the whole life time of the stressed material under a certain environment.

$$da/dt = AKI^n \quad (6)$$

where da/dt is the crack growth rate, A and n are crack-growth parameters, and KI is a stress intensity factor. Combining the inert strength distribution (=fast fracture strength), expressed by multimodal Weibull function (Eq.(3)), with above slow crack growth law, we can obtain the distribution functions of static and cyclic fatigue life and of dynamic fatigue strength.

For simplicity, in the following, suppose that $\sigma_{ui} = 0$. Let $\sigma_1 (> 0)$ be the maximum principal stress at any point of the material, and

is expressed by

$$\sigma = \dot{\sigma} \cdot g(r) t = \sigma_m \cdot g(r) \quad (7)$$

where r is a position vector, $\dot{\sigma}$ is a constant stress rate, σ_m is a representative stress (e.g. the maximum stress), $g(r)$ is a non-dimensional scalar function of the position vector, t is a time. Then, the risks of rupture for dynamic fatigue strength can be expressed by the following equations[7].

$$B_i = (\sigma_m / \sigma_{oi})^{m_i'} [A_{eff}]_i \quad (8)$$

where m_i and σ_{oi} are "mapped" Weibull parameters given by

$$m_i' = \frac{n_i + 1}{n_i - 2} m_i, \quad \sigma_{oi}' = \sigma_{oi} [\beta_i (n_i + 1) \dot{\sigma}]^{\frac{1}{n_i - 2}}, \quad \beta_i = 2 [(n_i - 2) A Y^2 K_{Ic}^{n_i - 2}]^{-1} \quad (9)$$

Here, $[A_{eff}]_i$ is a nondimensional effective volume, surface area or length of edges, expressed as

$$[A_{eff}]_i = \int_{A_i} g(r)^{n_i m_i / (n_i - 2)} dA_i \quad (10)$$

where A_i represents the domain of the i -th fracture cause and dA_i is an infinitesimal volume, surface or line element.

Figure 3 shows the Weibull plots of the bending strength of steatite ceramics under the constant stress rate $\dot{\sigma} = 2,74 \text{ MPa/sec}$ by using mean rank method (surface flaws). The dotted line (three-point bend, in air) and the broken line (four-point bend, in vacuum) in the figure are the theoretical curves calculated from Eqs.(2),(8) and (9). These curves coincide fairly well with the experimental results.

Almost the same stream line, we obtain the risks of rupture for cyclic fatigue life of ceramics. In this case, we suppose that the maximum principal stress at any point of the material is periodic and can be written by

$$\sigma = \sigma_m \cdot g(r) \cdot h(\omega t), \quad \omega: \text{angular velocity} \quad (11)$$

where $h(\omega t)$ is a function of ωt , for example, a sine wave. Then, the risk of rupture of cyclic fatigue life, N_{rep} , is expressed as [8]

$$B_i = (N_{rep}/N_{oi})^{m_{Ni}} \cdot [A_{eff}]_i \quad (12)$$

where m_{Ni} and N_{oi} are also "mapped" Weibull parameters given by

$$m_{Ni} = \frac{1}{n_i - 2} \cdot m_i \quad (13)$$

$$N_{oi} = \frac{B_i}{\sigma_m^{n_i} \int_0^{2\pi/\omega} h(\omega t)^{n_i} dt} \cdot \sigma_{oi}^{n_i - 2}$$

2.2 Two variables

Let introduce a random-variable vector

$$X = (\sigma_m, \xi)$$

where σ_m is a representative stress (inert strength) and ξ a fracture location. According to Oh and Finnie[9], when a body is subjected to a representative stress in a range $(\sigma_m, \sigma_m + d\sigma_m)$ and fails at a location ξ by i -th fracture cause, the joint probability density function $h_{A_i}(\sigma_m, \xi)$ can be written as

$$h_{A_i}(\sigma_m, \xi) d\xi d\sigma_m = \exp(-B_i) \frac{\partial}{\partial \sigma_m} (G_i) d\xi d\sigma_m \quad (14)$$

where A_i is a domain of i -th fracture cause, B_i is the risk of rupture due to i -th fracture cause and G_i is a function of B_i and ξ . Then B_i and G_i for Weibull's uniaxial distribution function can be written as

$$B_i = \int_{\xi} G_i d\xi, \quad G_i = \left(\frac{\sigma_i - \sigma_{ui}}{\sigma_{oi}} \right)^{m_i} \cdot Y(\sigma, \sigma_{ui}) \left(\frac{dA_i}{d\xi} \right) \quad (15)$$

where $Y(\cdot)$ is Heaviside's step function.

Combining Eq.(14) with the competing risk theory expressed by Eq.(1), the joint probability density function $h_A(\sigma_m, \xi)$ involving K fracture causes can be formulated as [10]

$$h_A(\sigma_m, \xi) = \prod_{i=1}^K R_i(\sigma_m) \cdot \sum_{j=1}^K \lambda_j \quad (16)$$

where R_i and λ_j are given as

$$R_i(\sigma_m) = 1 - \int_0^{\sigma_m} \int_{\xi_t} h_{Ai}(\sigma_m, \xi) d\xi d\sigma_m, \quad (17)$$

$$\lambda_j = h_{Aj}(\sigma_m, \xi) / R_j(\sigma_m), \quad A = A_1 \oplus A_2 \oplus \dots \oplus A_k.$$

Here, \int_{ξ_t} represents the integration over the total domain of A_i ; the \oplus symbol indicates "direct sum" used in set theory.

From Eqs.(16) and (17), two important marginals can be derived. The marginal with respect to fracture stress σ_m coincides with the multimodal Weibull distribution function. The other marginal with respect to fracture location ξ is of the so-called mixture type.

Analysis of diagnostic data of HP-Si₃N₄

Ito et al.[11] carried out the 3-point bending test to 415 HP-Si₃N₄ specimens (specimens had the following characteristics: mean grain size=2.0 μ m, surface roughness R_{max} =0.8 μ m, half span L =10.0mm, width b =1.5mm, half height h =1.5mm).

They measured the fracture stress σ_m , the coordinates of the fracture location (x, y) and the flaw size which initiated fracture. Using these fracture stress data, the bi-modal Weibull parameters m_i and σ_{0i} ($i=1$ for inner flaw, $i=2$ for surface flaw) have been estimated utilizing the multimaximum likelihood method (see next chapter) as shown in Table 1.

Using the estimated parameters in Table 1, we can estimate the distributions of fracture location, modified fracture stress and flaw size. Now we adopt the coordinate systems as shown in Fig.4.

Suppose that there are two types of fracture origin, namely,

inner cracks ($i=1$, the domain is expressed by A_1) and surface cracks ($i=2$, the domain is expressed by A_2), and that fracture does not occur at the side surfaces of a specimen.

The cumulative distribution function of the fracture location along the x axis $SA_1 \oplus A_2$ is derived below in Eq.(18); the function along the y axis $UA_1 \oplus A_2$ may be derived in a similar fashion, the result being shown in Eq.(19).

$$S_{A_1 \oplus A_2}(X) = S_{A_1}(X) \cdot P_{A_1} + S_{A_2}(X) \cdot P_{A_2}$$

$$SA_1(X) = (X/L)^{m_1+1}, \quad S_{A_2}(X) = (X/L)^{m_2+1} \quad (18)$$

$$PA_1 = \int_0^{\infty} dB_1/d\sigma_m \cdot \exp(-B_1 - B_2) d\sigma_m, \quad PA_2 = \int_0^{\infty} dB_2/d\sigma_m \cdot \exp(-B_1 - B_2) d\sigma_m$$

$$UA_1 \oplus A_2(Y) = U_{A_1}(Y) \cdot P_{A_1} + U_{A_2}(Y) \cdot P_{A_2}$$

$$U_{A_1}(Y) = 1 - \{(h-y)/h\}^{m_1+1}, \quad U_{A_2}(Y) = 1. \quad (19)$$

In Eqs.(18) and (19) p_{A_1} and p_{A_2} represent the cumulative fracture probabilities up to $\sigma_m = \infty$ in the domains A_1 and A_2 , respectively. Thus, Eqs.(18) and (19) are of the so-called mixture type. Therefore we can separate the date of fracture location simply. In Eqs.(18), note that the relation between $\ln SA_i(X)$ and $\ln(X/L)$ is linear.

The solid lines in Figs.5(a) and (b) show the individual distribution functions of fracture location calculated from Eq.(18). It can be seen that they coincide fairly well with the experimental data points, expressed by the + signs. Fig.6 shows the experimentally derived histogram relating to the y -coordinate of the depth of fracture origin. O signs connected by solid lines represent the estimated results calculated from Eq.(19); these coincide satisfactorily with the experimental results.

Distribution of Flaw Size

Suppose that the inner flaw which initiates fracture is a penny shaped crack parallel to y-z plane and that the following equation is valid, at fracture, for any crack size.

$$K_{Ic} = \frac{2}{\pi} \sigma_c \sqrt{\pi d/2} \quad (20)$$

where d is the diameter of the crack. Then we obtain

$$h\Lambda_1(d, \xi) = b_{m_1} \left(\frac{K_{Ic} \sqrt{\pi}}{\sqrt{2\sigma_{01}}} \right)^{m_1} d^{-(m_1+2)/2} \cdot \exp \left\{ -V_{e01} \left[\frac{K_{Ic} \sqrt{\pi}}{\sqrt{2\sigma_{01}}} \frac{Lh}{x(h-y)\sqrt{d}} \right]^{m_1} \right\} \quad (21)$$

From this equation, we can calculate the probability density function of the crack size d as a marginal.

Fig.7 shows the histogram of observed flaw size d. In this figure, o signs connected with solid lines represent the theoretical results ($K_{Ic}=4.06 \text{ MPa}\sqrt{\text{m}}$); these coincide precisely with experimental results within the range of comparatively large crack size (40-85 μm).

Although the observed crack size at mode (about 35 μm) coincides with that of the estimated one, the absolute value of percentage is different. It would appear that this difference results from the assumption that K_{Ic} value is dependent of the crack size/mean grain size ratio.

Recently it was found that the fracture toughness of ceramics decreases as the ratio of the crack size versus the mean grain-size does. Usami et al.[12] deduced the following equation to explain such phenomena.

$$K_c/K_{Ic} = \frac{(1+r/2 a_e)^{1/2}}{(1+r/a_e)} \quad (22)$$

where K_{Ic} is the plane strain fracture toughness obtained from comparatively large cracks; K_c is an apparent fracture toughness for a small crack; r is the size of the weakest grain (which is taken to be twice the mean grain-size); $2a_e$ is a size of an

equivalent two-dimensional straight crack. Since we assumed that there are penny shaped cracks in a body, a_e in our case is given by

$$a_e \leq 0.2dc$$

Substituting K_c given by Eq.(22) into K_{Ic} in Eq.(21), we obtain the joint probability density function under three-point bending load[13].

Closed circles (\bullet signs) are the calculated results obtained from the above analysis, which coincide with the experimental results better than those of open circles (\circ signs). However, the calculated results expressed by ! signs over-estimate the flaw-size in the region $dc > 50\mu\text{m}$. Therefore, from the view point of the structural reliability, the analysis using K_{Ic} is better than that using Eq.(22).

2.3 Three variables

In the theory explained in section 2.2, we supposed that the penny-shaped crack which might cause fracture should lie perpendicular to the maximum principal stress. However, the crack which may cause fracture does not always lie as thus. If we want to know the flaw-orientation distribution as well as those of fracture stress, flaw-size and flaw location, we have to adopt the multi-axial Weibull distribution function instead of uni-axial one.

Let introduce a random-variable vector as

$$x = (\sigma_m, \xi, \alpha) \quad (23)$$

then we obtain the three-variable joint probability density

function as [14].

$$h_{Ai}(\sigma_m, \xi, \alpha) d\alpha d\xi d\sigma_m = \exp(-B_i) \frac{\partial}{\partial \sigma_m} (G_i) d\alpha d\xi d\sigma_m, \quad (24)$$

$$B_i = \int_{\xi_t} \int_{\alpha_t} G_i d\alpha d\xi, \quad G_i = \frac{1}{2\pi} \left(\frac{Z_i - \sigma_{ui}}{\sigma_{ei}} \right)^{m_i} \gamma(Z_i, \sigma_{ui}) \left(\frac{d\hat{A}}{d\alpha} \right) \left(\frac{dA_i}{d\xi} \right).$$

where, the subscript t means the total domain of each variable; $d\hat{A}$ is a surface element of a unit sphere. In general, α is a 2-dimensional vector which has two independent components related to the space angles, say θ and ϕ (see Fig.8).

Similar to Eq.(16), the joint probability density function $h_A(\sigma_m, \xi, \alpha)$ involving K causes of fracture can be formulated as

$$h_A(\sigma_m, \xi, \alpha) = \prod_{i=1}^K R_i \cdot \sum_{j=1}^K \lambda_j,$$

$$R_i = 1 - \int_0^{\sigma_m} \int_{\xi_t} \int_{\alpha_t} h_{Ai}(\sigma_m, \xi, \alpha) d\alpha d\xi d\sigma_m, \quad (25)$$

$$\lambda_i = h_{Ai}(\sigma_m, \xi, \alpha) / R_i,$$

$$A = A_1 \oplus A_2 \oplus \dots \oplus A_K.$$

Equation (25) is valid for an arbitrary stress state and arbitrary types of fracture origins.

Using the general equation derived in the above, we analyse the 3-point bending test of a rectangular cross-sectioned ceramic specimen (see Fig.4).

For simplicity, we suppose that there is only one type of fracture origin, namely, penny-shaped crack. For the first step, we employ the shear insensitive criteria as a mixed mode fracture criteria.

In the analysis it is assumed that the crack plane is perpendicular to the thickness direction of a specimen. Therefore, $d\alpha = d\phi$.

The distribution function of flaw-orientation is obtained as the marginal with respect to flaw-orientation angle ϕ as

$$H_{A1}(\phi) = 1 - \cos^{2m_i+1} \phi \quad (26)$$

which leads to the following density function.

$$h_{A1}(\phi) = (2m_1 + 1) \sin\phi \cdot \cos^{2m_1}\phi \quad (27)$$

Fig.9 shows the calculated flaw-orientation distribution function and the density function. From these figures we see that the flaw-orientation distribution shifts toward low angle and becomes sharp as m value increases. These mean that the smaller the scatterness of fracture strength becomes, the smaller the flaw-orientation angle does. It is without saying that the probability density function is strongly influenced by the fracture criteria[14]. The analysis mentioned above, including those of the previous section, may play an important role on non-destructive inspection of ceramic component[15].

3. Estimation of Weibull Parameters

One of the most important factors in statistical analysis using multimodal Weibull distribution may be the problem as to how accurately the parameters can be estimated, how accurate the parameters obtained are, and how many samples are necessary. The method for estimating Weibull parameters is outlined below.

Multimodal-Weibull distribution contains a number of parameters (m_i , σ_{oi} , σ_{ui}). It is known that although, by the nature of its mathematical structure, we can estimate parameters of multimodal-Weibull distribution by directly maximizing the likelihood function, its estimation accuracy is very low. However, its accuracy can be raised significantly by using fracture cause data [16]. If parameters can be estimated with such high accuracy, the information thus obtained can be fed back

to material design.

Multistep maximum-likelihood method

According to competing risk theory, the likelihood function for data (complete data) on known strength and fracture causes, which are known to conform to the multimodal-Weibull distribution, is given by [16,17]:

$$L = \text{Const.} \times \prod_{i=1}^k L_i, \quad L_i = \left[\prod_{j=1}^{n_i} f_i(x_{ij}) \right] \quad (28)$$

$$\left[\prod_{j=1}^{n_i} R_i(x_{ij}) \right],$$

$$R_i = \exp(-B_i), \quad f_i = B_i' \exp(-B_i)$$

where i : type of fracture cause, n_i : number of test pieces fractured by fracture cause i and X_{ij} ($i=1, \dots, k; j=1, \dots, n_i$): strength data for j th of test pieces fractured by fracture causes i . L_i in the above equation contains only single-distribution f_i . Thus, a set of parameters which maximize L_i is the maximum likelihood estimates. With $\sigma_{0i}=0$, each maximum likelihood equation is expressed by

$$\sigma_{0i} = \left(\frac{A_{eff}}{n_i} \sum_{j=1}^{n_i} x_j^{m_i} \right)^{1/m_i}, \quad \frac{n_i}{m_i} + \sum_{j=1}^{n_i} \ln x_j - n_i \frac{\sum_{j=1}^{n_i} x_j^{m_i} \cdot \ln x_j}{\sum_{j=1}^{n_i} x_j^{m_i}}, \quad \eta = \sum_{i=1}^k n_i \quad (29)$$

Thus m_i and σ_{0i} can be obtained. This is called a multistep maximum-likelihood method.

Ito et al.[11] conducted an HP-Si3N4 (3x3x28mm) 3-point bending test, as mentioned previously, producing the following results: 326 internally fractured, 77 surface fractured and 12 undetermined from total of 415 test pieces. Figure 10 shows the results of Weibull plotting of the above results[10] in accordance with fracture causes by using the Johnson method[18]. The solid line in the figure is a theoretical curve calculated by using parameter estimates ($m_1=15.79$, $\sigma_{01}=95.99$, $m_2=12.73$ and

$\sigma_0=129.5$) obtained by the multistep maximum likelihood method. It agrees well with the values measured.

In addition, with some unknown fracture cause data involved, the parameters can still be estimated with high accuracy by using the improved EM algorithm[16].

Relationship Between Distribution of Parameter Estimates and Number of Samples

Let us write the maximum-likelihood estimates for parameters m and ξ contained in multimodal Weibull distribution function as \hat{m} and $\hat{\xi}$, respectively. It is known that if the number n of samples is large, the distribution of \hat{m}/m conforms to a normal one with mean 1 and variance: $0.608/n$. For example, with $n=25$ or 50, the coefficient of variation for \hat{m} is as follows:

$$n=25 : \text{cov} = \sqrt{\frac{0.608}{25}} = 0.156$$

$$n=50 : \text{cov} = \sqrt{\frac{0.608}{50}} = 0.110$$

Thus, with the coefficient of variation for \hat{m} necessary for designing given, the necessary number of samples can be determined.

If the number of samples is small, the distribution of estimates, both unimodal- and multimodal- Weibull distributions, can be known only by using Monte Carlo simulation.

4. Conclusions

The generalised multimodal Weibull function, which is a function of a random variable vector, was presented by combining the competing risk theory and fracture mechanics. Three special cases were shown; the first are the distribution functions of

fast-fracture strength, dynamic fatigue strength and cyclic fatigue life as the case which has only one random variable (one dimensional case); the second are those of fracture stress and fracture location or crack size at fracture origin as the case which has two random variables (two dimensional case); the third has three-random variables, namely, fracture strength, fracture location and flaw-orientation (three-dimensional case). The calculated results satisfactorily coincided with the experimental results carried out on HP-Si₃N₄ by Ito et al..

References

1. M.L.Moeschberger and H.A.David, *Biometrics*,27,909(1971).
2. Y.Matsuo, *Engineering Fracture Mechanics*,14,527(1981).
- 3.Y.Matsuo,preprintof the JSME,780-4,15(1978).*Trans.JSME(A)*,46,605(1980).
4. Y.Matsuo, *Bulletin of the JSME*,26,1461(1983).
- 5.Y.Matsuo,T.Ogasawara,S.Kimura and E.Yasuda, *J. Mater. Sci.*,22,1482(1987).
6. Y.Matsuo,T.Ogasawara,E.Yasuda and S.Kimura, *Proc.of Int. Symp. on Machining of Advanced Ceramic Materials and Components*,Pittsburg,235(1987).
7. Y.Matsuo,E.Yasuda and S.Kimura, *Proc.4th Int.Structural safety and Reliability*,Kobe,II-461(1985).
8. Y.Matsuo, T.Oida, K.Jinbo, K.Yasuda and S.Kimura, *J.Ceram.Soc. Japan*,97,136(1989).
9. H.L.Oh and I.Finnie, *Int.J.Fracture*,6,287(1970).
- 10.Y.Matsuo and K.Kitakami, in *Fracture Mechanics of Ceramics*,7 (Eds. R.C.Bradt et al.),Plenum Pub.,223(1986).
- 11.S.Ito,et al., *Proc.25th Japan Congress on Materials Research* (1982).
- 12.S.Usami,et al., *Preprint of Soc.Mater.Sci.Japan*,159(1984).
- 13.Y.Matsuo,K.Kitakamiand S.Kimura,*J.Ceram.Soc.Japan*,94,711(1986)

14. Y. Matsuo, K. Kitakami and S. Kimura, Proc. Int. Inst. Sci. Sintering (IISS) Symp., Tokyo, (Eds. S. Somiya et al.), 802 (1987).
15. Y. Matsuo, K. Kitakami and S. Kimura, J. Mater. Sci., 22, 2253 (1987).
16. H. Murata, Y. Matsuo, M. Miyakawa and K. Kitakami, Trans. the JSME(A), 52, 27 (1986).
17. M. R. Samford, Biometrics, 8, 307 (1952).
18. L. G. Johnson, The Statistical Treatment of Fatigue Experiment, Elsevier (1964).

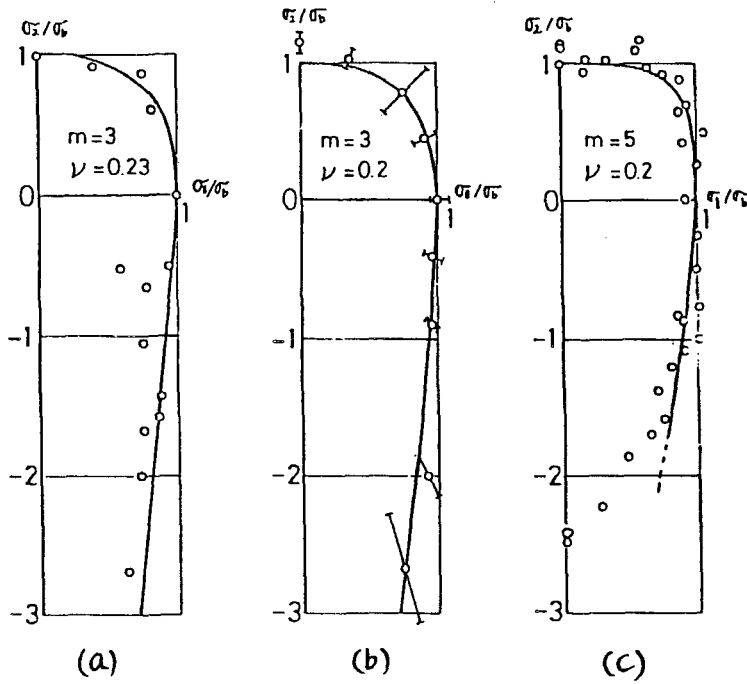


Fig.1 Fracture loci under bi-axial stress state (a)Alumina by S.M.Broutman et al.(1972), (b) Graphite by R.Ely (1965), (c) Cast iron by I.Cornet and R.C.Grassi (1955). The solid lines are calculated from Eq.(4).

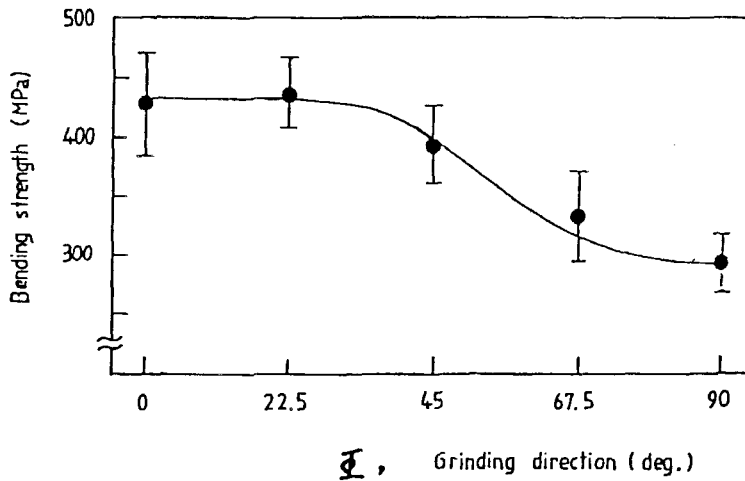


Fig.2 Effect of the grinding direction on 4-point bending strength and expected value calculated from Eq.(4).

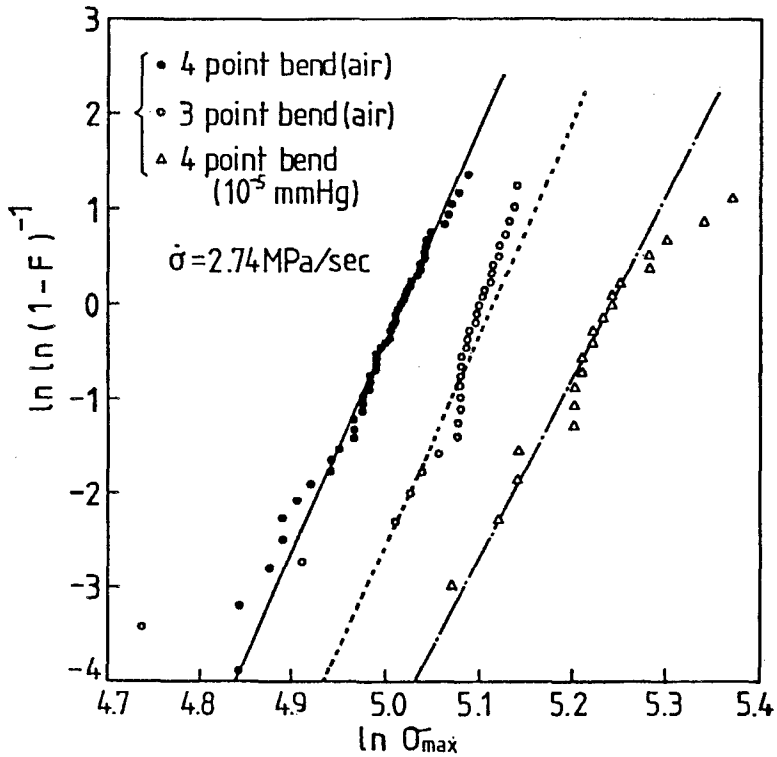


Fig.3 Weibull plots of the experimental results on steatite ceramics under the stress rate $\dot{\sigma} = 2.74 \text{ MPa/sec}$.

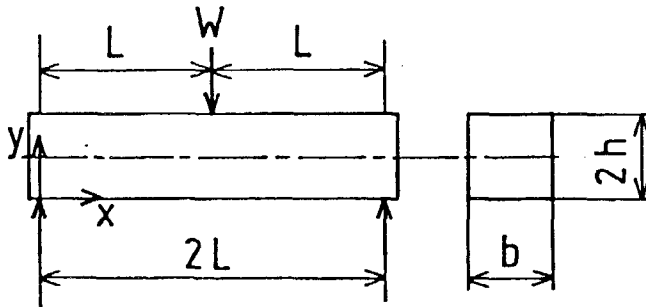


Fig.4 A rectangular cross-sectioned specimen subjected to the 3-point bending load and the coordinate systems.

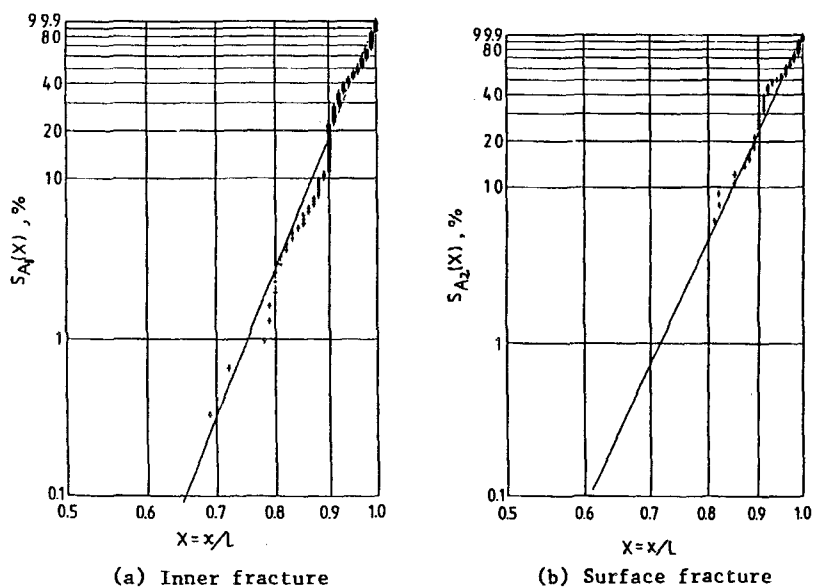


Fig.5 Plots of the fracture probability $S(x)$ and the fracture location ratio x/L on log-log scale graph paper. The solid lines are the estimated values calculated from Eq. (18) (HP-Si N [11]).

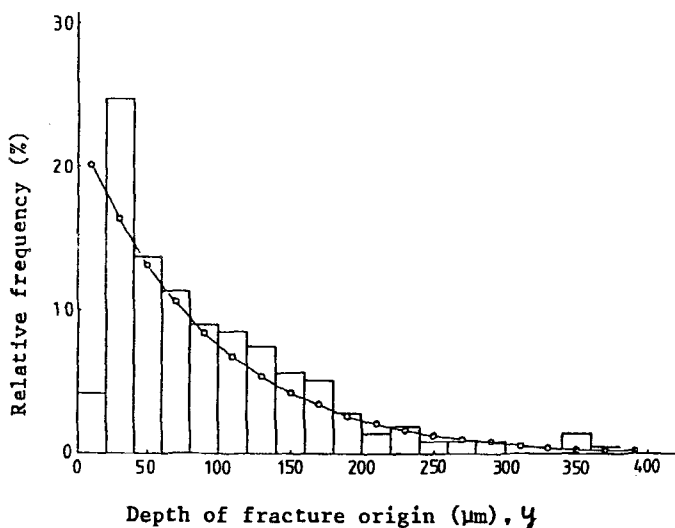


Fig.6 Histogram of the depth of inner fracture origin relating to the y -coordinate (HP-Si N [11], o signs are the calculated results from Eq.(19).

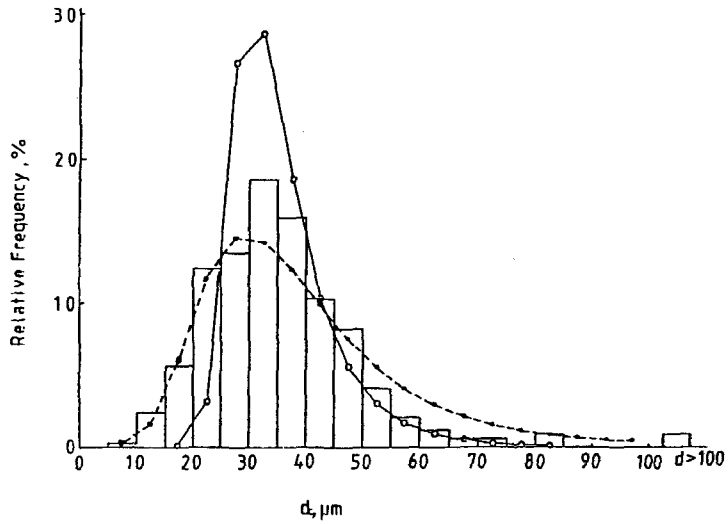


Fig.7 Histogram of flaw-size for 3-point bending of HP-Si N [11] (o signs: $K_c=K_{Ic}$, o signs: Eq.(22)).

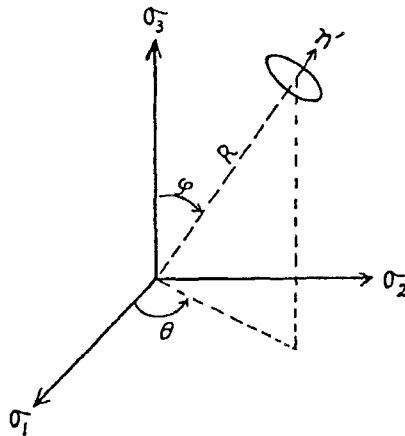


Fig.8 Coordinate systems used in the analysis

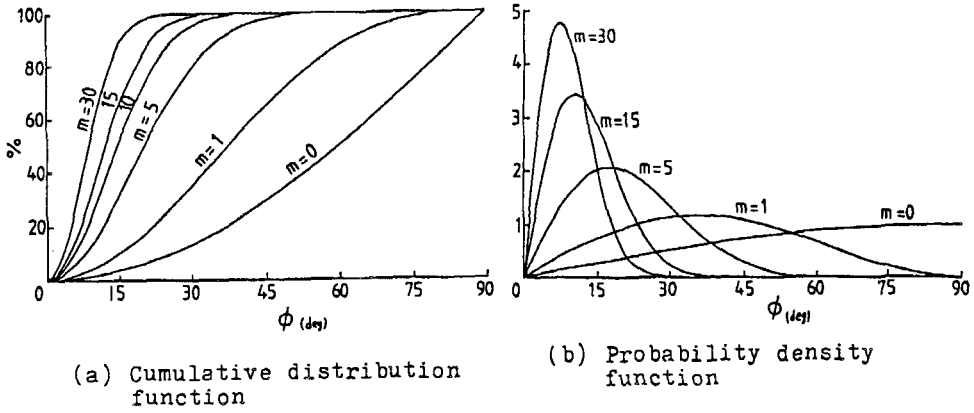


Fig.9 Flaw-orientation distribution (shear insensitive)

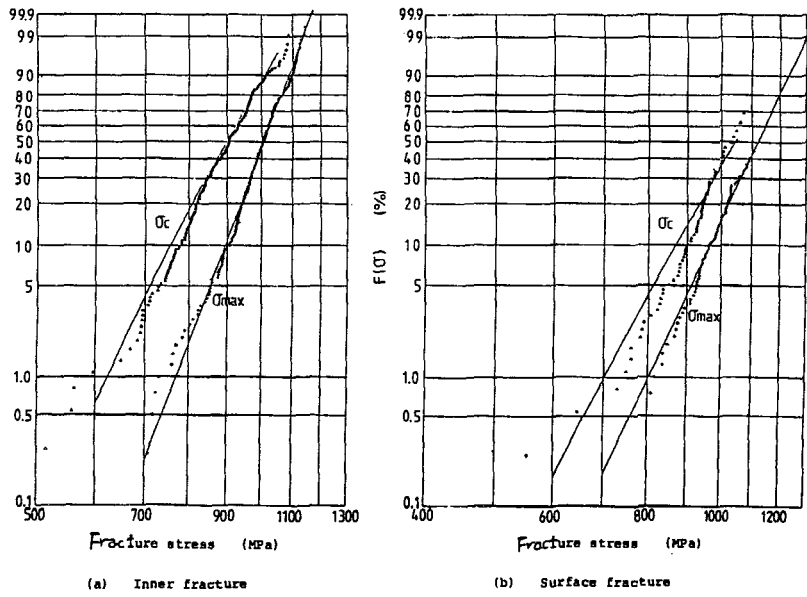


Fig.10 Weibull plots of the fracture stress σ_{max} (HP-Si N [11]) according to Johnson method[18]. The solid lines are the calculated results using competing risk theory. σ_c is a corrected fracture stress at fracture origin, which can be estimated from Eq.(16).

Table 1. Weibull parameters estimated by the multi-maximum likelihood method (M-MLE).

	\hat{m}_i	$\hat{\sigma}_{0i}$
Inner fracture (i=1)	15.79	959.9
Surface fracture (i=2)	12.73	1295